Article

Development of Porous Polyacrylonitrile Composite Fibers: New Precursor Fibers with High Thermal Stability

Ehsan Samimi-Sohrforozani [1], Sara Azimi [1], Alireza Abolhasani [2], Samira Malekian [1], Shahram Arbab [3], Mahmoud Zendehdel [4,5], Mohammad Mahdi Abolhasani [1,*] and Narges Yaghoobi Nia [5,*]

1. Chemical Engineering Department, University of Kashan, Kashan 8731753153, Iran; Ehsansamimi2022@gmail.com (E.S.-S.); Sa.azimi1987@gmail.com (S.A.); Samira_malekian@yahoo.com (S.M.)
2. Civil Engineering Department, University of Kashan, Kashan 8731753153, Iran; Abolhasani1991@gmail.com
3. Department of Textile Engineering, ATMT Research Institute, Amirkabir University of Technology, Tehran 1591634311, Iran; Shahram.arbab@aut.ac.ir
4. Kimia Solar Research Institute, Kimia Solar Company, Kashan 8713745868, Iran; m.zendehdel@kimiasolar.com
5. Centre for Hybrid and Organic Solar Energy (CHOSE), University of Rome Tor Vergata, 00133 Rome, Italy
* Correspondence: abolhasani@kashanu.ac.ir (M.M.A.); YAGHOOBI.NIA@ing.uniroma2.it (N.Y.N.)

Abstract: Polyacrylonitrile (PAN) fibers with unique properties are becoming increasingly important as precursors for the fabrication of carbon fibers. Here, we suggest the preparation of porous PAN composite fibers to increase the homogeneity and thermal stability of the fibers. Based on the thermodynamics of polymer solutions, the ternary phase diagram of the PAN/H_2O/Dimethylformamide (DMF) system has been modeled to introduce porosity in the fibers. Adding a conscious amount of water (4.1 wt.%) as a non-solvent to the PAN solution containing 1 wt.% of graphene oxide (GO), followed by wet spinning, has led to the preparation of porous composite fibers with high thermal stability and unique physicochemical properties. Differential scanning calorimetry (DSC) and thermogravimetric analysis (TGA) results elucidate that PAN/GO/H_2O porous composite fibers have a higher thermal decomposition temperature, increased residual weight, reduced heat release rate, and higher crystallinity in comparison with the pristine PAN fibers, being a promising precursor for the development of high-performance carbon fibers. The results show a promising application window of the synthesized PAN fibers in electronic and electrochemical devices.

Keywords: polyacrylonitrile composite fiber; porous fibers; phase diagram; high crystallinity; thermal stability

1. Introduction

Carbon fibers have been considered as promising materials for a large number of applications in the automotive industry, motorsports, and turbine blade manufacturing due to their light weight, stiffness, and extraordinary properties [1,2]. Polyacrylonitrile (PAN) fibers with high crystallinity, excellent thermal stability, and other remarkable characteristics are widely utilized as primary precursors in manufacturing high-performance carbon fibers [3–5].

Among various polymer fiber fabrication techniques, wet spinning and electrospinning have been the most frequently applied methods in the recent years [6–22]. Known as a primary method, wet spinning has been employed to prepare a significant majority of PAN fibers [23–26]. In addition, numerous researches have focused on the modification of PAN precursor fibers since the quality of carbon fibers entirely depends on the physical and structural properties of the precursor such as crystallinity and thermal stability [3,27].

The inclusion of various fillers such as clay, cellulose nanocrystal, carbon allotropes, and other nanoparticles (MoS_2, TiO_2, Fe_3O_4) into the structure of fibers has been widely conducted to modify PAN fibers [28–38]. For instance, PAN composite fibers containing graphene oxide (GO) have gained significant interest owing to their large surface

area and the effect of the functional groups of filler, which result in appropriate inter-actions with polymer [39,40]. Zhao et al. [41] provided PAN/GO composite fibers with enhanced thermal stability by increasing the amount of graphene oxide up to 3 wt.%. PAN/functionalized graphene composite fibers have demonstrated improved thermal properties as the corresponding heat release rate peak decreased by 36.7% compared to pristine PAN fibers [42]. Papkov et al. [43] introduced 1.4 wt.% of GO to the PAN solution, leading to an increment in the graphitic order of the final carbon nanofibers by increasing the carbonization temperature. The gel-spinning approach has also been employed to fabricate a porous PAN/GO composite with higher crystallinity [39].

As an alternative approach to modify PAN precursors, low-density fibers can be fabricated to develop light carbon fibers for high-performance structures. To fulfil this goal, recent studies have designed porosity in PAN fibers [33,44].

Here, we offer an elegant method to prepare porous PAN composite fibers with enhanced physical properties through studying the thermodynamics of polymer solu-tions and the physics of polymer/solvent/anti-solvent interaction along with the ad-dition of nanofiller. To introduce porosity in the fibers, the ternary phase diagram of PAN/H_2O/DMF system is modeled using the Flory–Huggins theory, and then 4.1 wt.% of water as non-solvent is added to the PAN solution containing 1 wt.% of GO. The cloud points of the ternary system are also determined experimentally and are in good agreement with the obtained theoretical phase diagram. The as-spunned PAN/GO/H_2O composite fibers demonstrate higher crystallinity, a reduction in heat release rate, and grow thin thermal decomposition temperatures as well as residual weight compared to the pristine PAN fibers. Such outstanding outcomes confirm the excellent homogenous structure and thermal stability of the resulting fibers, which are of great importance for the fabrication of lightweight and high-performance carbon fibers.

2. Materials and Methods

2.1. Materials

Poly(acrylonitrile-*ran*-methylacrylate) (94 wt.% of acrylonitrile monomer, M_n = 36,000 g/mol, M_v = 70,000 g/mol, M_w = 116,000 g/mol, and PDI = 3.2) was purchased from Polyacryl Company, Isfahan, Iran. GO nanoparticle (thickness of 3.4–7.0 nm) was obtained from USNANO, Houston, TX, USA. Dimethylformamide (DMF) was supplied from Merck, Darmstadt, Germany.

2.2. Preparation of PAN Fibers

Four solutions were prepared for the wet spinning according to Table 1. For prepa-ration of blank sample (dope A), a specific amount of PAN powder (14.4 gr) was added into 108 mL DMF to make an initial spinning dope for the wet spinning system, and it was stirred overnight at 45 °C. For dope B, H_2O (4.8 mL) and DMF (103.2 mL) were mixed and stirred for 30 min at room temperature. Then, PAN (14.26 gr) was added to the solution and stirred overnight at 45 °C. In the case of dope C, GO (0.14 gr) was sonicated in DMF (108 mL) for 1 h to make a homogeneous dark solution. Subsequently, PAN was added to the solution and stirred overnight at 45 °C. Dope D was prepared by mixing defined amounts of H_2O (4.8 mL), DMF (103.2 mL) and GO (0.14 gr) in the solution. Following this, PAN powder was swelled in the resultant solution and stirred overnight at 45 °C. It is to be noted that for the determination of cloud points, PAN/DMF solutions with different concentrations of 5, 8, 10, and 15 wt.% PAN was first prepared. Afterward, water was added slowly to the PAN/DMF solution till the initial solution turned turbid. The doped polymers were spun into the fibers using wet spinning system method. A metering pump (pump constant = 0.5 cm^3/rev) extruded the dopes at same shear rate (16,000 1/s) into a 1-m-long coagulation bath containing tap water at 25 °C. The process was carried out through a single-hole spinneret with a diameter of 200 µm and L/D of 2.

Table 1. Description of PAN-based fibers.

Dope	GO (wt%)	H_2O (wt%)	Sample Code
A	0	0	PAN
B	0	4.1	PAN/H_2O
C	1	0	PAN/GO
D	1	4.1	PAN/GO/H_2O

2.3. Characterization

2.3.1. Field Emission Scanning Electron Microscope (FE-SEM)

Cross-sectional images of as-spun fibers were obtained using a MIRA3 TESCAN microscope (Brno-Kohoutovice, Czech Republic). All samples were freeze-fractured in liquid nitrogen. Then, a thin layer of gold was coated on the fractured surfaces to be observed with FE-SEM.

2.3.2. High Resolution Transmission Electron Microscopy (HR-TEM)

The morphology of wet spun fibers was imaged by an HR-TEM (FEI Tecnai F20, Hillsboro, OR, USA) operated at 200 kV.

2.3.3. Fourier Transform Infrared Spectroscopy (FTIR)

FTIR spectra of the samples were obtained in a range between 500 and 4000 cm^{-1} using the KBr pellets on a Magna 550 Nicolet spectrometer (Waltham, MA, USA).

2.3.4. Differential Scanning Calorimetry (DSC)

DSC analysis was performed on a Mettler Toledo calorimeter (Strategy Tower 1, Singapore) through heating the samples from 25 °C to 400 °C at a rate of 10 °C/min under N_2 atmosphere.

2.3.5. X-ray Diffraction (XRD)

XRD pattern of samples was recorded using an X-ray diffractometer (Panalytical Company, Almelo, Netherlands) equipped with Cu K$_\alpha$ radiation (40 kV, 30 mA).

2.3.6. Thermogravimetric Analysis (TGA)

In order to study thermal stability of the fibers, TGA was carried out using a BAHR thermal analyzer (model STA 503, Hüllhorst, Germany) at a heating rate of 10 °C/min in the temperature range of 25–800 °C under a constant flow of argon environment.

3. Results

3.1. Ternary Phase Diagram

The porosity within the wet spun fibers is accurately outlined using the thermodynamics and kinetics of liquid–liquid phase separation in the ternary mixture of PAN, solvent (DMF), and H_2O (non-solvent). Achieving a correlation between PAN fiber morphology and initial H_2O content is in no way trifling. To gain further intuition into phase behavior, the ternary phase diagram of PAN/H_2O/DMF was constructed using the Flory–Huggins theory. Details of the model are presented in Note 1 in the Supporting Information. The calculated ternary phase diagram is shown in Figure 1. For clarity, the cloud points and tie lines are shown by the blue squares and black dashes, respectively. The obtained binodal fits the experimental cloud points excellently, confirming our approach.

In the next step, we aimed to determine the percentage of water related to the critical points. At such points, the polymer dopes move from the miscible region to the unstable region without passing through the metastable region, leading to spontaneous liquid–liquid demixing and the formation of an interpenetrating bicontinuous structure. Interestingly, the resulting as-spun fibers are homogeneous and have suitable properties [45]. On the

other hand, a high percentage of non-solvent in the dope results in the formation of fibers with low porosity [46]. Thus, 4.1 wt.% of water as a non-solvent was added to the polymer dope, which is close to the critical point.
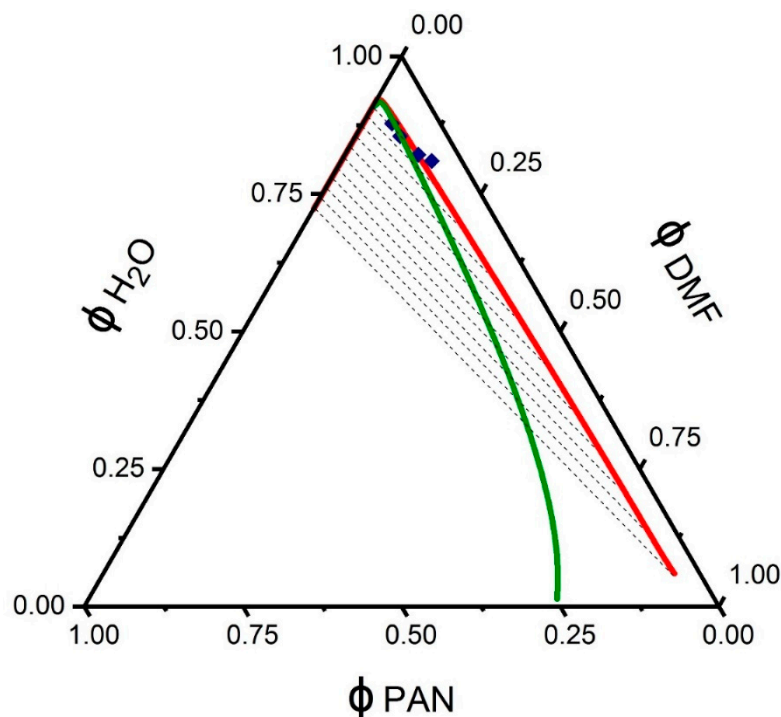

Figure 1. Obtained ternary phase diagram for PAN/H_2O/DMF. The binodal curve has been fitted against experimentally determined cloud point compositions (blue squares). The spinodal curve and tie lines are indicated in green and gray, respectively.

3.2. Morphological Analysis of PAN-Based Fibers

Cross-sectional FE-SEM images of different PAN fibers are illustrated in Figure 2. Pristine PAN fibers with a diameter of 277 µm have porosity and micrometric voids due to the presence of water as the coagulating agent in the coagulation bath during the wet spinning process [47]. FE-SEM images show that in the presence of H_2O, its concentration enrichment lowered overall fiber porosity. In PAN/H_2O fibers (d = 504 µm), a diminished thermodynamic affinity toward mass transfer between H_2O and fiber precursor emerges, which decreases the numbers of micrometric channels compared to the pristine PAN fibers [46]. However, the number of finger-like channels with decreased width increased. PAN/GO composite fiber (d = 312 µm) has the same cross-sectional structure as pristine PAN fiber and no noticeable change in the channels or voids of fibers appeared. The cross-section FE-SEM image of PAN/GO/H_2O (d = 319 µm) shows that the micrometric channels and holes protect the center of the fibers. Additionally, the number of finger-like channels enhances from the center to the outer surface of the fibers.

The HR-TEM image of the PAN/GO/H_2O composite fiber and the corresponding SAED pattern are shown in Figure 3. The SAED pattern reveals continuous circles, originating from the crystalline nature of GO. The observed rings are related to the planes of GO with "d" spacing of 1.2 Å and 2.1 Å [48], suggesting the presence of GO inside the composite fiber.
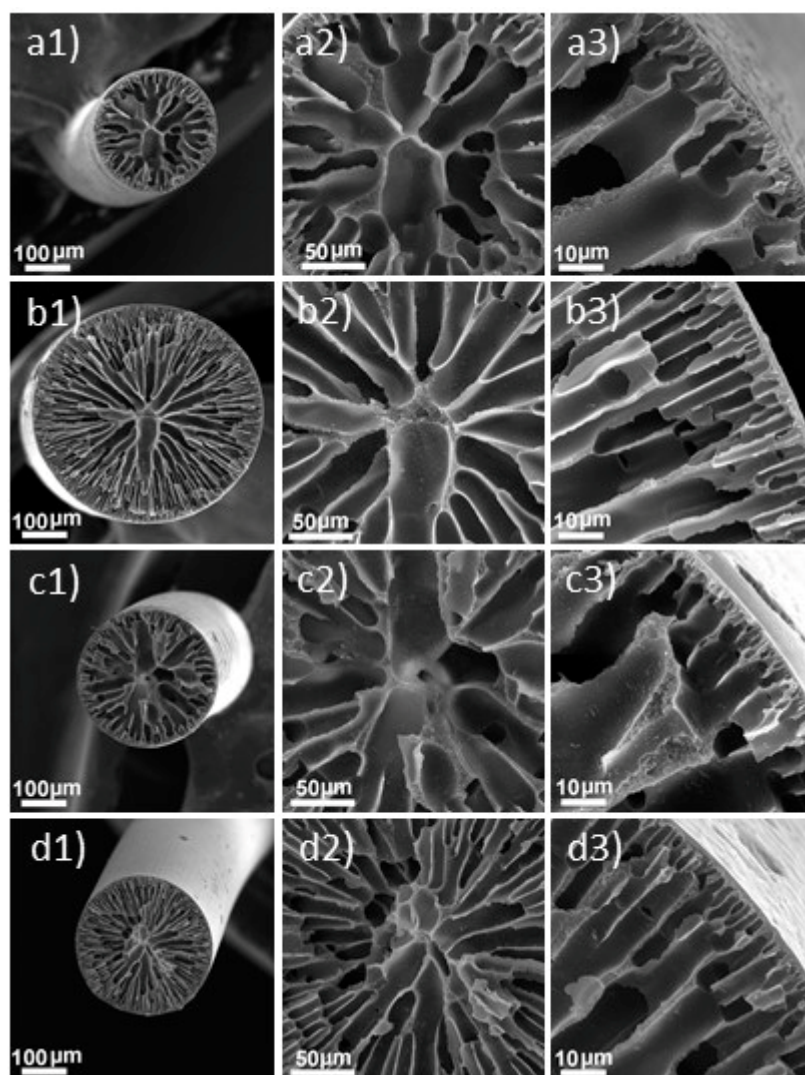
Figure 2. SEM images of fiber cross-section; (**a1**–**a3**) pristine PAN fibers, (**b1**–**b3**) PAN/H$_2$O fibers, (**c1**–**c3**) PAN/GO composite fibers, and (**d1**–**d3**) PAN/GO/H$_2$O composite fibers.
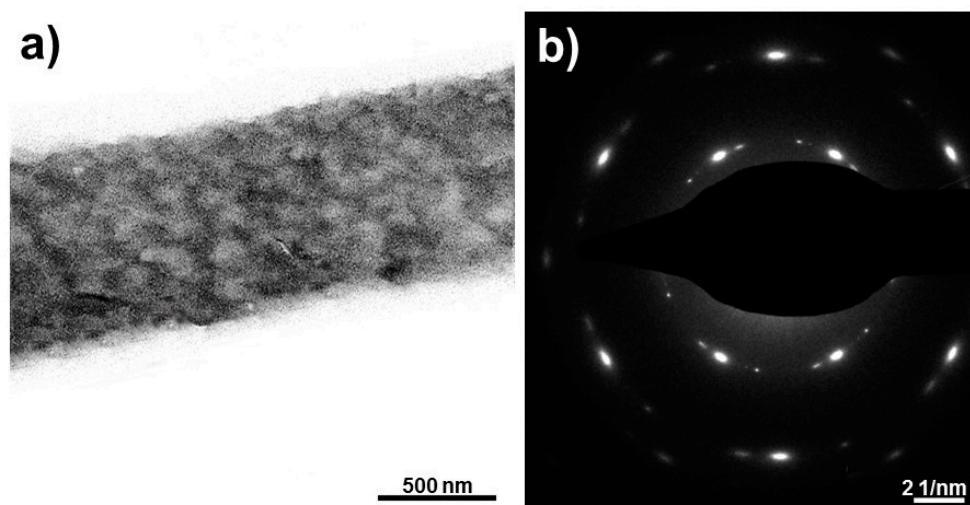

Figure 3. (**a**) HR-TEM image and (**b**) corresponding SAED pattern of PAN/GO/H$_2$O composite fiber.

3.3. Structural Analysis of PAN-Based Fibers

FTIR spectra of the PAN-based fibers are represented in Figure 4a. The band in the range of 2850–2950 cm^{-1} is attributed to the stretching vibration modes of CH and CH_2 groups of PAN chains and the characteristic band at 2244 cm^{-1} is delineated to the stretching vibration of nitrile (C≡N). The absorption bands at 1631 cm^{-1} and 1732 cm^{-1} are related to C=C and C=O bonds, respectively [49]. Moreover, the C-O stretching band in the methyl acrylate monomer structure appears in the range of 1255–1090 cm^{-1} [50–52]. In the FTIR spectra of PAN/H_2O and PAN/GO composite fibers, the intensity of bonds increased compared to that of the $PAN/GO/H_2O$ composite fiber, which could be related to the bond polarity. As illustrated in Figure 4b, hydroxyl groups of H_2O and GO can form H-bonding with the nitrile group of PAN chain that enhances the nitrile bond polarity. However, in the case of $PAN/GO/H_2O$ composite fiber, this polarity decreases since H_2O has more affinity to interact with GO rather than PAN.
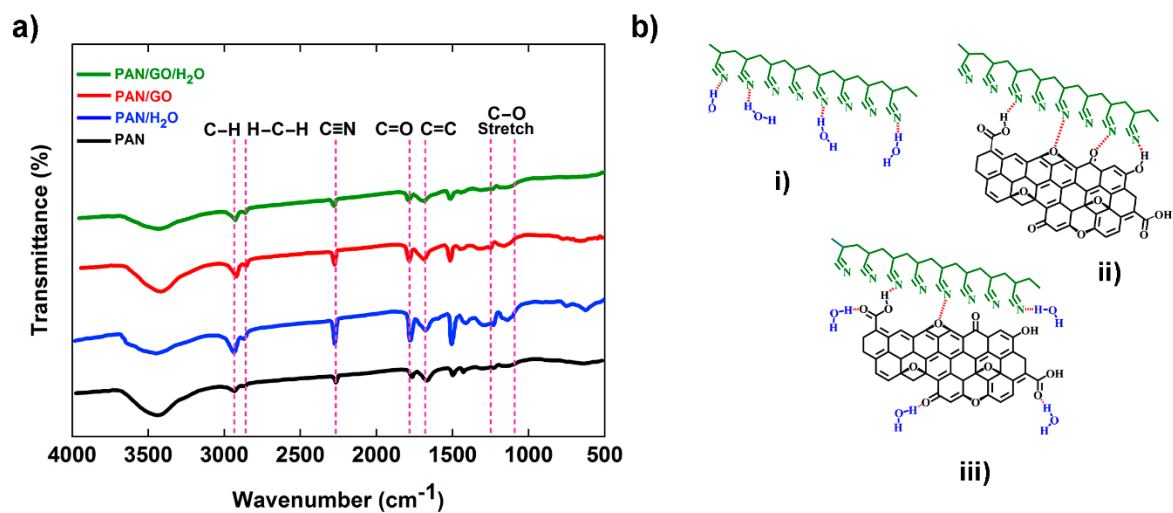

Figure 4. (**a**) FTIR spectra of PAN-based fibers, (**b**) Schematic of the interaction in (i) PAN/H_2O composite fiber, (ii) PAN/GO composite fiber, and (iii) $PAN/GO/H_2O$ composite fiber.

XRD patterns of PAN-based fibers reveal a sharp and a small peak at 2θ angle of ~17° and ~27°, which are related to the crystalline and amorphous regions in the fibers, respectively (Figure 5) [25,53]. Crystallinity of the pristine PAN fiber, PAN/H_2O composite fiber, PAN/GO composite fiber, and $PAN/GO/H_2O$ composite fiber were obtained as 19.4%, 21.6%, 25.6%, and 26%, respectively, using the corresponding XRD patterns. The presence of GO with a layered structure during the composite fiber gelation process leads to higher crystallinity of the fiber as it can enforce the alignment of polymer chains [54]. Results suggest that the addition of a non-solvent along with filler resulted in the formation of PAN precursor fibers with augmented crystallinity, which can improve the graphite order and mechanical properties of the final carbon fibers [55,56].
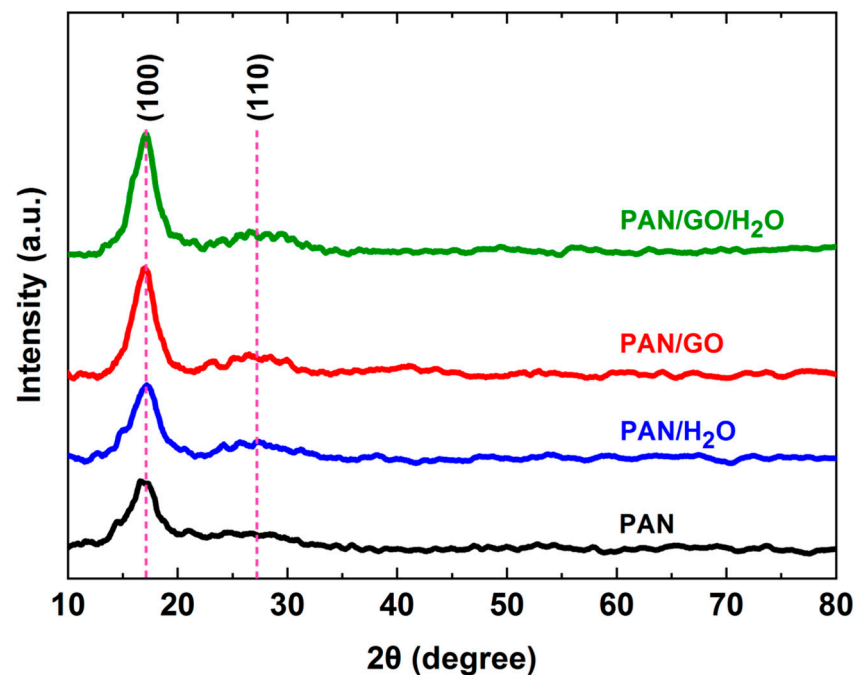
Figure 5. XRD patterns of PAN-based fibers.

3.4. Thermal Behavior of PAN-Based Fibers

DSC thermograms of the fibers are demonstrated in Figure 6 and their relevant parameters have been summarized in Table 2. For the pristine PAN fibers, an exothermic peak temperature (T_P) appeared at 308.4 °C, related to the typical cyclization reaction of PAN [57,58]. The PAN/H_2O, PAN/GO, and PAN/GO/H_2O composite fibers showed peak temperatures at 297.6, 295.1, and 294.6 °C, respectively. Due to the addition of H_2O to the PAN fiber, the T_P decreased by 10.75 °C compared to the pristine PAN fiber. Additionally, for the PAN/GO composite fiber, a decline of 13.31 °C was observed for the exothermic peak temperature since acidic functional groups can decline the cyclization temperature and the released heat by ionic interactions between GO and PAN [59]. Interestingly, the most change in the exothermic peak temperature occurs in the presence of both H_2O and GO. Results illustrate that the incorporation of H_2O and GO in the PAN fibers decreases the required activation energy for initiation cyclization reaction, reducing T_P [60]. In addition, such a reduction in T_P can help avoid extreme heat eruptions and obtain a homogeneous stabilized structure in the prepared composite fibers [61]. The exothermic rate parameter ($\Delta H/\Delta T$) was also calculated for each sample from the DSC thermograms (Table 2). It was found that the parameter decreased by 31.2% and 49.2% for PAN/H_2O and PAN/GO composite fiber, respectively, in comparison with pristine PAN fiber. However, a significant reduction (51.6%) was obtained in $\Delta H/\Delta T$ when both H_2O and GO were introduced into the PAN fibers, confirming that our integrated technique was successful in diminishing the amount of released heat in less time for the fiber. As a consequence, the as-prepared, modified PAN-based composite fiber had a homogeneous stabilized structure with less decomposition of polymer chains and high graphitic order, which are vital for manufacturing high-performance carbon fibers [43,62].
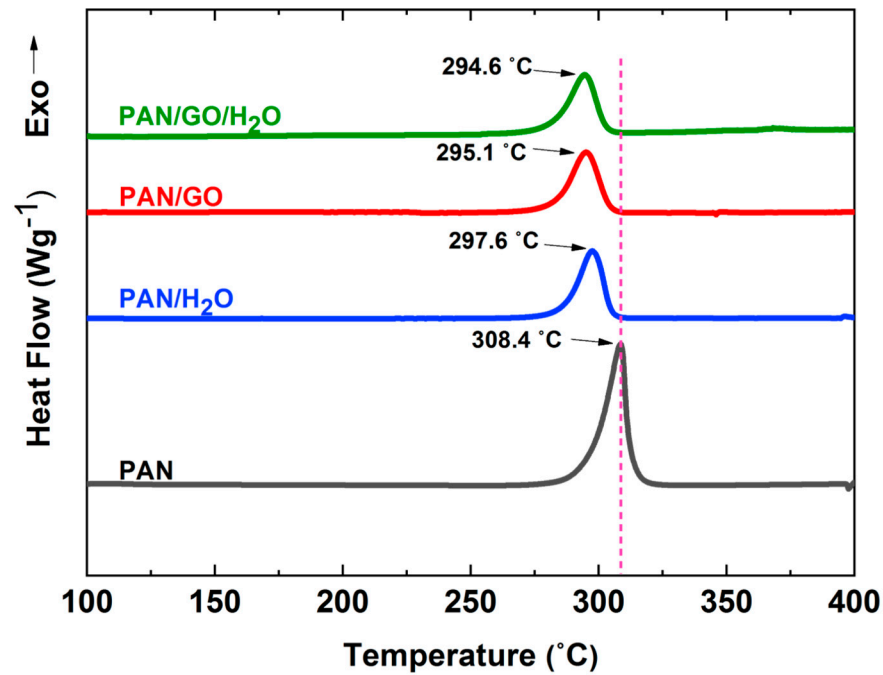
Figure 6. DSC thermograms of PAN-based fibers.

Table 2. DSC parameters of PAN-based fibers.

Sample Fiber	T_i (°C)	T_P (°C)	T_f (°C)	ΔT (°C)	ΔH (Wg^{-1})	$\Delta H/\Delta T$ (Wg$^{-1}\cdot$°C^{-1})
PAN	271.5	308.4	328.1	56.6	7.26	0.128
PAN/H$_2$O	270.1	297.6	310.6	40.5	3.57	0.088
PAN/GO	260.6	295.1	310.2	49.6	3.24	0.065
PAN/GO/H$_2$O	254.9	294.6	309.4	54.5	3.41	0.062

TGA curves of the PAN-based fibers are observed in Figure 7a and the corresponding parameters are listed in Table 3. For all samples, the first main weight loss starts around 50 °C, which can be attributed to the loss of water molecules and low molecular weight oligomers [63]. DTG curves show a thermal decomposition temperature (T_d) of 299.4 °C for pristine PAN fibers (Figure 7b). Through the addition of water and nanofiller to the fibers, the temperature reached 302.6 and 302.8 °C for PAN/H$_2$O fiber and PAN/GO composite fibers, respectively. However, T_d increased to a high temperature of 307.1 °C for PAN/GO/H$_2$O composite fibers. It is worth noting that decomposition, which happens above ~300 °C, is assigned to backbone degradation of the pristine PAN fibers [41]. Thus, the PAN backbone decomposition temperature was notably enhanced for the PAN/GO/H$_2$O composite fibers. The layered structures of GO may function as cross-bonding points and contribute to a vital interaction between polymer chains and nanofillers, resulting in a highly intensified thermal stability [64]. Moreover, the weight loss in T_d was calculated as 10.1%, 9.5%, 5.1%, and 2.2% for pristine PAN fibers, PAN/H$_2$O fibers, PAN/GO composite fibers, and PAN/GO/H$_2$O composite fibers, respectively, demonstrating high thermal stability of the PAN/GO/H$_2$O composite fibers among other samples [42]. The residual weight percentages of the samples were also attained at 800 °C ignoring the weight of evaporated H$_2$O in the water-containing fibers. This parameter reached 33.8% for the pristine PAN fiber; however, it increased to 35.0%, 47.2%, and 48.2% for PAN/H$_2$O fiber, PAN/GO composite fibers, and PAN/GO/H$_2$O composite fibers, respectively. High residual weight percentages of the modified PAN/GO/H$_2$O composite fibers originate from high thermal stability of the sample [42,65]. Additionally, it can be seen that com-

pared to previous studies, notable results have been obtained in our study (Table S3). As a consequence, the promising approach presented here is an effective strategy to produce modified precursor PAN fibers with unique properties, which helps the fabrication of high-performance carbon fibers.
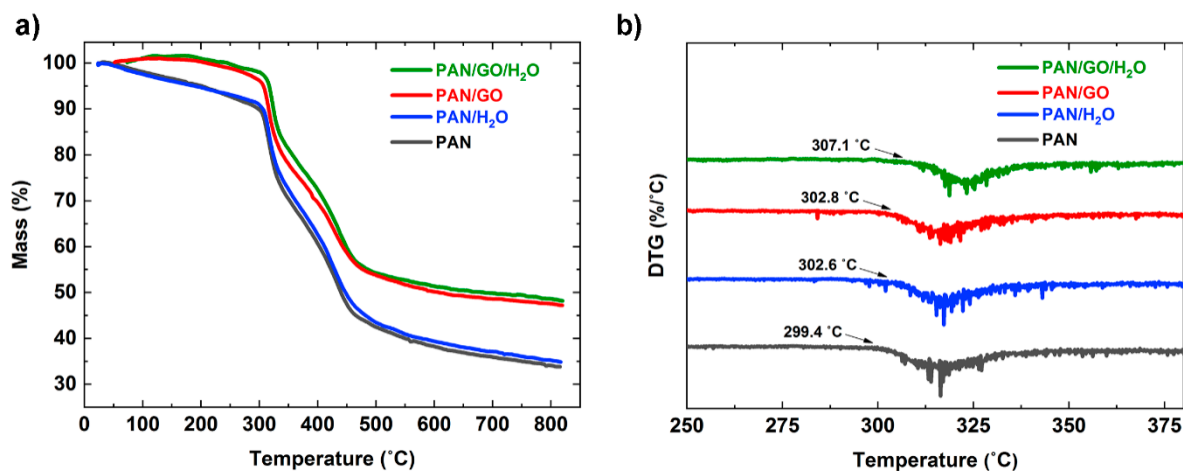

Figure 7. (**a**) TGA and (**b**) DTG curves of PAN-based fibers.

Table 3. Thermal properties of PAN-based fibers calculated from TGA and DTG curves.

Sample Fiber	T_d (°C)	Wight Loss at T_d (%)	Residual Weight at 800 °C (%)
PAN	299.4	10.1	33.8
PAN/H_2O	302.6	9.5	35.0
PAN/GO	302.8	5.1	47.2
PAN/GO/H_2O	307.1	2.2	48.2

4. Conclusions

In summary, we have prepared PAN precursor porous composite fibers by simultaneously adding nanofiller (GO) and non-solvent (H_2O), which are profoundly modified in thermal stability and properties. The ternary phase diagram of the PAN/H_2O/DMF system has been modeled using the Flory–Huggins theory to determine the non-solvent content and tailor porosity in the fibers. DSC results demonstrate higher crystallinity content and a more homogeneous stabilized structure of PAN/GO/H_2O composite fiber compared to pristine PAN fibers due to its reduced heat release rate. Our modification technique also results in the thermal stability of porous composite fibers confirmed by TGA. Thermal decomposition temperature and residual weight of PAN/GO/H_2O composite fibers has increased in comparison with pristine PAN fibers, giving a suitable precursor for the production of high-performance carbon fibers.

Author Contributions: Conceptualization, E.S.-S., S.A. (Sara Azimi), A.A., S.M., S.A. (Shahram Arbab), M.Z., M.M.A. and N.Y.N.; methodology, E.S.-S., S.A. (Sara Azimi), A.A., S.M., S.A. (Shahram Arbab), M.Z., M.M.A. and N.Y.N.; software, E.S.-S. and S.M.; validation, E.S.-S., S.A. (Sara Azimi), A.A., S.M., S.A. (Shahram Arbab), M.Z. and M.M.A.; formal analysis, E.S.-S. and S.M., investigation E.S.-S., S.A. (Sara Azimi), A.A., S.M., S.A. (Shahram Arbab), and M.M.A.; resources, M.M.A.; data

References

1. Edie, D.D. The effect of processing on the structure and properties of carbon fibers. *Carbon* **1998**, *36*, 345–362. [CrossRef]
2. Zabihi, O.; Ahmadi, M.; Li, Q.; Shafei, S.; Huson, M.G.; Naebe, M. Carbon fibre surface modification using functionalized nanoclay: A hierarchical interphase for fibre-reinforced polymer composites. *Compos. Sci. Technol.* **2017**, *148*, 49–58. [CrossRef]
3. Wangxi, Z.; Jie, L.; Gang, W. Evolution of structure and properties of PAN precursors during their conversion to carbon fibers. *Carbon* **2003**, *41*, 2805–2812. [CrossRef]
4. Morris, E.A.; Weisenberger, M.C.; Abdallah, M.G.; Vautard, F.; Grappe, H.; Ozcan, S.; Paulauskas, F.L.; Eberle, C.; Jackson, D.; Mecham, S.J.; et al. High performance carbon fibers from very high molecular weight polyacrylonitrile precursors. *Carbon* **2016**, *101*, 245–252. [CrossRef]
5. Fox, B. Making stronger carbon-fiber precursors. *Science* **2019**, *366*, 1314–1315. [CrossRef] [PubMed]
6. Nataraj, S.K.; Yang, K.S.; Aminabhavi, T.M. Polyacrylonitrile-based nanofibers-A state of the art review. *Prog. Polym. Sci.* **2012**, *37*, 487–513. [CrossRef]
7. Agarwal, S.; Greiner, A.; Wendorff, J.H. Functional materials by electrospinning of polymers. *Prog. Polym. Sci.* **2013**, *38*, 963–991. [CrossRef]
8. Abolhasani, M.M.; Naebe, M.; Amiri, M.H.; Shirvanimoghaddam, K.; Anwar, S.; Michels, J.J.; Asadi, K. Hierarchically structured porous piezoelectric polymer nanofibers for energy harvesting. *Adv. Sci.* **2020**, *7*, 2000517. [CrossRef]
9. Azimi, S.; Golabchi, A.; Nekookar, A.; Rabbani, S.; Amiri, M.H.; Asadi, K.; Abolhasani, M.M. Self-powered cardiac pacemaker by piezoelectric polymer nanogenerator implant. *Nano Energy* **2021**, *83*, 105781. [CrossRef]
10. Anwar, S.; Amiri, M.H.; Jiang, S.; Abolhasani, M.M.; Rocha, P.R.F.; Asadi, K. Piezoelectric nylon-11 fibers for electronic textiles, energy harvesting and sensing. *Adv. Funct. Mater.* **2020**, *31*, 2004326. [CrossRef]
11. Baqeri, M.; Abolhasani, M.M.; Mozdianfard, M.R.; Guo, Q.; Oroumei, A.; Naebe, M. Influence of processing conditions on polymorphic behavior, crystallinity, and morphology of electrospun poly(VInylidene fluoride) nanofibers. *Appl. Polym. Sci.* **2015**, *132*, 30. [CrossRef]
12. Jia, Z.; Lu, C.; Liu, Y.; Zhou, P.; Wang, L. Lignin/Polyacrylonitrile composite hollow fibers prepared by wet-spinning method. *ACS Sustain. Chem. Eng.* **2016**, *4*, 2838–2842. [CrossRef]
13. Fashandi, H.; Abolhasani, M.M.; Sandoghdar, P.; Zohdi, N.; Li, Q.; Naebe, M. Morphological changes towards enhancing piezoelectric properties of PVDF electrical generators using cellulose nanocrystals. *Cellulose* **2016**, *23*, 3625–3637. [CrossRef]
14. Abolhasani, M.M.; Shirvanimoghaddam, K.; Naebe, M. PVDF/graphene composite nanofibers with enhanced piezoelectric performance for development of robust nanogenerators. *Compos. Sci. Technol.* **2017**, *138*, 49–56. [CrossRef]
15. Mishra, R.K.; Mishra, P.; Verma, K.; Mondal, A.; Chaudhary, R.G.; Abolhasani, M.M.; Loganathan, S. Electrospinning production of nanofibrous membranes. *Environ. Chem. Lett.* **2018**, *17*, 767–800. [CrossRef]
16. Abolhasani, M.M.; Naebe, M.; Shirvanimoghaddam, K.; Fashandi, H.; Joordens, H.K.M.; Pipertzis, A.; Anwar, S.; Berger, R.; Floudas, G.; Michels, J.; et al. Thermodynamic approach to tailor porosity in piezoelectric polymer fibers for application in nanogenerators. *Nano Energy* **2019**, *62*, 594–600. [CrossRef]
17. Zhang, H.; Quan, L.; Gao, A.; Tong, Y.; Shi, F.; Xu, L. The structure and properties of polyacrylonitrile nascent composite fibers with grafted multi walled carbon nanotubes prepared by wet spinning method. *Polymers* **2019**, *11*, 422. [CrossRef]
18. Sun, L.; Shang, L.; Xiao, L.; Zhang, M.; Li, M.; Ao, Y. Structural changes of polyacrylonitrile fibers in the process of wet spinning. *Appl. Polym. Sci.* **2020**, *137*, 48905. [CrossRef]
19. Abolhasani, M.M.; Azimi, S.; Fashandi, H. Enhanced ferroelectric properties of electrospun poly (vinylidene fluoride) nanofibers by adjusting processing parameters. *RSC Adv.* **2015**, *5*, 61277–61283. [CrossRef]
20. Abolhasani, M.M.; Jalaei, A.; Tavana, R.; Kashani, F.Z. Processing and performance properties of amino silicone-based softener on various textile substrates. *Polym. Bull.* **2020**, *77*, 2557–2572. [CrossRef]

21. Abolhasani, M.M.; Shirvanimoghaddam, K.; Khayyam, H.; Moosavi, S.M.; Zohdi, N.; Naebe, M. Towards predicting the piezoelectricity and physiochemical properties of the electrospun P (VDF-TrFE) nanogenrators using an artificial neural network. *Polym. Test.* **2018**, *66*, 178–188. [CrossRef]

22. Soleymani, H.; Noormohammadi, M.; Kashi, M.A.; Amiri, M.H.; Michels, J.J.; Asadi, K.; Abolhasani, M.M. Self-Poled Sausage-Like PVDF nanowires produced by confined phase inversion as novel piezoelectric nanogenerators. *Adv. Mater. Interfaces* **2021**, *8*, 2001734. [CrossRef]

23. Chen, J.; Ge, H.-Y.; Dong, X.-G.; Wang, C.-G. The formation of polyacrylonitrile nascent fibers in wet-spinning process. *J. Appl. Polym. Sci.* **2007**, *106*, 692–696. [CrossRef]

24. Fakhrhoseini, S.M.; Khayyam, H.; Naebe, M. Chemically enhanced wet-spinning process to accelerate thermal stabilization of polyacrylonitrile fibers. *Macromol. Mater. Eng.* **2018**, *303*, 1700557. [CrossRef]

25. Al Faruque, M.A.; Remadevi, R.; Razal, J.; Wang, X.; Naebe, M. Investigation on structure and characteristics of alpaca-based wet-spun polyacrylonitrile composite fibers by utilizing natural textile waste. *Appl. Polym. Sci.* **2019**, *137*, 48370. [CrossRef]

26. Yang, H.-S.; Kim, Y.-M.; Choi, H.; Jang, J.; Youk, J.H.; Lee, B.-S.; Yu, W.-R. Electrochemical wet-spinning process for fabricating strong PAN fibers via an in situ induced plasticizing effect. *Polymer* **2020**, *202*, 2641. [CrossRef]

27. Liu, Y.; Kumar, S. Recent progress in fabrication, structure, and properties of carbon fibers. *Polym. Rev.* **2012**, *52*, 234–258. [CrossRef]

28. Liu, Y.; Chae, H.G.; Kumar, S. Gel-spun carbon nanotubes/polyacrylonitrile composite fibers. Part III: Effect of stabilization conditions on carbon fiber properties. *Carbon* **2011**, *49*, 4487–4496. [CrossRef]

29. Gao, Q.; Ma, H.; Bao, W.; Gao, C.; Ge, M. Polyacrylonitrile/electroconductive TiO$_2$ nanoparticles composite fibers via wet-spinning. *Fibers Polym.* **2016**, *17*, 1048–1054. [CrossRef]

30. Hiremath, N.; Mays, J.; Bhat, G. Recent developments in carbon fibers and carbon nanotube-based fibers: A Review. *Polym. Rev.* **2016**, *57*, 339–368. [CrossRef]

31. Elagib, T.H.H.; Hassan, E.A.M.; Fan, C.; Han, K.; Yu, M. Microwave pre-oxidation for polyacrylonitrile precursor coated with nano-carbon black. *Polym. Eng. Sci.* **2019**, *59*, 457–464. [CrossRef]

32. Chang, H.; Luo, J.; Liu, H.C.; Zhang, S.; Park, J.G.; Liang, Z.; Kumar, S. Stabilization study of polyacrylonitrile/cellulose nanocrystals composite fibers. *ACS Appl. Polym. Mater.* **2019**, *1*, 1015–1021. [CrossRef]

33. Liu, H.C.; Luo, J.; Chang, H.; Davijani, A.A.B.; Wang, P.-H.; Kumar, S. Polyacrylonitrile sheath and polyacrylonitrile/lignin core bi-component carbon fibers. *Carbon* **2019**, *149*, 165–172. [CrossRef]

34. Sun, J.; Ge, Q.; Guo, L.; Yang, Z. Nitrogen doped carbon fibers derived from carbonization of electrospun polyacrylonitrile as efficient metal-free HER electrocatalyst. *Int. J. Hydrog. Energy* **2020**, *45*, 4035–4042. [CrossRef]

35. Zhang, C.-L.; Jiang, Z.-H.; Lu, B.-R.; Liu, J.-T.; Cao, F.-H.; Li, H.; Yu, Z.-L.; Yu, S.-H. MoS$_2$ nanoplates assembled on electrospun polyacrylonitrile-metal organic framework-derived carbon fibers for lithium storage. *Nano Energy* **2019**, *61*, 104–110. [CrossRef]

36. Dai, Z.; Ren, P.-G.; Jin, Y.-L.; Zhang, H.; Ren, F.; Zhang, Q. Nitrogen-sulphur Co-doped graphenes modified electrospun lignin/polyacrylonitrile-based carbon nanofiber as high performance supercapacitor. *Power Sources* **2019**, *437*, 226937. [CrossRef]

37. Benko, A.; Nocuń, M.; Gajewska, M.; Błażewicz, M. Addition of carbon nanotubes to electrospun polyacrylonitrile as a way to obtain carbon nanofibers with desired properties. *Polym. Degrad. Stab.* **2019**, *161*, 260–276. [CrossRef]

38. Cao, Z.; Li, W.; Sou, X.; Liu, Y.; Lu, C. Structures and cyclization behaviors of gel-spun cellulose/polyacrylonitrile composite fibers. *Polym. Test.* **2020**, *81*, 106276. [CrossRef]

39. Chien, A.T.; Liu, H.C.; Newcomb, B.A.; Xiang, C.; Tour, J.M.; Kumar, S. Polyacrylonitrile fibers containing graphene oxide nanoribbons. *ACS Appl. Mater. Interfaces* **2015**, *7*, 5281–5288. [CrossRef] [PubMed]

40. Mottaleb, M.M.A.; Mohamed, A.; Karim, S.A.; Osman, T.A.; Khattab, A. Preparation, characterization, and mechanical properties of polyacrylonitrile (PAN)/graphene oxide (GO) nanofibers. *Mech. Adv. Mater. Struct.* **2018**, *27*, 346–351. [CrossRef]

41. Zhao, R.; Tian, M.; Zhao, Y.; Chen, S.; Han, G. Wet-spinning assembly of continuous and macroscopic graphene oxide/polyacrylonitrile reinforced composite fibers with enhanced mechanical properties and thermal stability. *Appl. Polym. Sci.* **2019**, *136*, 46950. [CrossRef]

42. Qiu, M.; Wang, D.; Zhang, L.; Li, M.; Liu, M.; Fu, S. Simultaneously electrochemical exfoliation and functionalization of graphene nanosheets: Multifunctional reinforcements in thermal, flame-retardant, and mechanical properties of polyacrylonitrile composite fibers. *Polym. Compos.* **2020**, *41*, 1561–1573. [CrossRef]

43. Papkov, D.; Goponenko, A.; Compton, O.C.; An, Z.; Moravsky, A.; Li, X.-Z.; Nguyen, S.T.; Dzenis, Y.A. Improved graphitic structure of continuous carbon nanofibers via graphene oxide templating. *Adv. Funct. Mater.* **2013**, *23*, 5763–5770. [CrossRef]

44. Gulgunje, P.V.; Newcomb, B.A.; Gupta, K.; Chae, H.G.; Tsotsis, T.K.; Kumar, S. Low-density and high-modulus carbon fibers from polyacrylonitrile with honeycomb structure. *Carbon* **2015**, *95*, 710–714. [CrossRef]

45. Tan, L.; Pan, D.; Pan, N. Thermodynamic study of a water-dimethylformamide-polyacrylonitrile ternary system. *Appl. Polym. Sci.* **2008**, *110*, 3439–3447. [CrossRef]

46. Arbab, S.; Noorpanah, P.; Mohammadi, N.; Soleimani, M. Designing index of void structure and tensile properties in wet-spun polyacrylonitrile (PAN) fiber. I. Effect of dope polymer or nonsolvent concentration. *Appl. Polym. Sci.* **2008**, *109*, 3461–3469. [CrossRef]

47. Takahashi, M.; Nukushina, Y.; Kosugi, S. Effect of fiber-forming conditions on the microstructure of acrylic fiber. *Text. Res.* **1964**, *34*, 87–97. [CrossRef]

48. Saxena, S.; Tyson, T.A.; Shukla, S.; Negusse, E.; Chen, H.; Bai, J. Investigation of structural and electronic properties of graphene oxide. *Appl. Phys. Lett.* **2011**, *99*, 013104. [CrossRef]

49. Korobeinyk, A.V.; Whitby, R.L.D.; Mikhalovsky, S.V. High temperature oxidative resistance of polyacrylonitrile-methylmethacrylate copolymer powder converting to a carbonized monolith. *Eur. Polym. J.* **2012**, *48*, 97–104. [CrossRef]

50. Haris, M.R.H.M.; Kathiresan, S.; Mohan, S. FT-IR and FT-Raman spectra and normal coordinate analysis of poly methyl methacrylate. *Der Pharma Chem.* **2010**, *2*, 316–323.

51. Singhal, A.; Dubey, A.; Bhardwaj, Y.K.; Jain, D.; Choudhury, S.; Tyagi, A.Y. UV-shielding transparent PMMA/In2O3 nanocomposite films based on In_2O_3 nanoparticles. *RSC Adv.* **2013**, *3*, 43. [CrossRef]

52. Tucureanu, V.; Matei, A.; Mihalache, I.; Danila, M.; Popescu, M.; Bita, B. Synthesis and characterization of YAG:Ce,Gd and YAG:Ce,Gd/PMMA nanocomposites for optoelectronic applications. *Mater. Sci.* **2014**, *50*, 1883–1890. [CrossRef]

53. Jin, J.; Ogale, A.A. Carbon fibers derived from wet-spinning of equi-component lignin/polyacrylonitrile blends. *Appl. Polym. Sci.* **2018**, *135*, 45903. [CrossRef]

54. Guo, Z.; Wang, M.; Huang, Z.-H.; Kang, F. Preparation of graphene/carbon hybrid nanofibers and their performance for NO oxidation. *Carbon* **2015**, *87*, 282–291. [CrossRef]

55. Liu, F.; Wang, H.; Xue, L.; Fan, L.; Zhu, Z. Effect of microstructure on the mechanical properties of PAN-based carbon fibers during high-temperature graphitization. *Mater. Sci.* **2008**, *43*, 4316–4322. [CrossRef]

56. Gutmann, P.; Will, J.M.; Kurt, S.; Xu, Y.; Horn, S. Carbonization of polyacrylonitrile-based fibers under defined tensile load: Influence on shrinkage behavior, microstructure, and mechanical properties. *Polym. Degrad. Stab.* **2019**, *163*, 174–184. [CrossRef]

57. Kim, J.; Kim, Y.C.; Ahn, W.; Kim, C.Y. Reaction mechanisms of polyacrylonitrile on thermal treatment. *Polym. Eng. Sci.* **1993**, *33*, 1452–1457. [CrossRef]

58. Zhao, W.; Lu, Y.; Wang, J.; Chen, Q.; Zhou, L.; Jiang, J.; Chen, L. Improving crosslinking of stabilized polyacrylonitrile fibers and mechanical properties of carbon fibers by irradiating with γ-ray. *Polym. Degrad. Stab.* **2016**, *133*, 16–26. [CrossRef]

59. Kaur, J.; Millington, K.; Cai, J.Y. Rheology of polyacrylonitrile-based precursor polymers produced from controlled (RAFT) and conventional polymerization: Its role in solution spinning. *Appl. Polym. Sci.* **2016**, *133*, 48. [CrossRef]

60. Bose, S.; Kuila, T.; Uddin, M.E.; Kim, N.H.; Lau, A.K.T.; Lee, J.H. In-situ synthesis and characterization of electrically conductive polypyrrole/graphene nanocomposites. *Polymer* **2010**, *51*, 5921–5928. [CrossRef]

61. Ouyang, Q.; Wang, X.; Wang, X.; Huang, J.; Huang, X.; Chen, Y. Simultaneous DSC/TG analysis on the thermal behavior of PAN polymers prepared by aqueous free-radical polymerization. *Polym. Degrad. Stab.* **2016**, *130*, 320–327. [CrossRef]

62. Liu, H.; Zhang, S.; Yang, J.; Ji, M.; Yu, J.; Wang, M.; Chai, X.; Yang, B.; Zhu, C.; Xu, J. Preparation, stabilization and carbonization of a novel polyacrylonitrile-based carbon fiber precursor. *Polymers* **2019**, *11*, 1150. [CrossRef] [PubMed]

63. Zhang, H.; Quan, L.; Gao, A.; Tong, Y.; Shi, F.; Xu, L. Thermal analysis and crystal structure of poly(acrylonitrile-co-itaconic acid) copolymers synthesized in water. *Polymers* **2020**, *12*, 221. [CrossRef]

64. Wang, Q.; Li, G.; Zhang, J.; Huang, F.; Lu, K.; Wei, Q. PAN nanofibers reinforced with MMT/GO hybrid nanofillers. *J. Nanomater.* **2014**, *2014*. [CrossRef]

65. Qiao, M.; Kong, H.; Ding, X.; Zhang, L.; Yu, M. Effect of graphene oxide coatings on the structure of polyacrylonitrile fibers during pre-oxidation process. *RSC Adv.* **2019**, *9*, 28146–28152. [CrossRef]